Yield surface approximation for lower and upper bound yield design of 3d composite frame structures

Jérémy Bleyer, Patrick de Buhan

Yield surface approximation for lower and upper bound yield design of 3D composite frame structures

Jeremy Bleyer[a,*], Patrick de Buhan[a]

[a] *Université Paris-Est, Laboratoire Navier,*
Ecole des Ponts ParisTech-IFSTTAR-CNRS (UMR 8205)
6-8 av Blaise Pascal, Cité Descartes, 77455 Champs-sur-Marne, FRANCE

Abstract

The present contribution advocates an up-scaling procedure for computing the limit loads of spatial structures made of composite beams. The resolution of an auxiliary yield design problem leads to the determination of a yield surface in the space of axial force and bending moments. A general method for approximating the numerically computed yield surface by a sum of several ellipsoids is developed. The so-obtained analytical expression of the criterion is then incorporated in the yield design calculations of the whole structure, using second-order cone programming techniques. An illustrative application to a complex spatial frame structure is presented.

Keywords: yield design, limit analysis, composite frames, yield surface approximation, second-order cone programming, finite element method

1. Introduction

The computation of structural limit loads using limit analysis or, in a more general manner, yield design theory, relies on performing mathematical programming techniques. Until recently, efficient interior-point algorithms were only available for linear programming (LP) problems. For this reason, many authors have treated yield design problems numerically, using piecewise linearization of the material yield surface to obtain LP problems [1, 33, 36–38]. It should also be mentioned that piecewise linearization has also been advantageously used for a wide range of elasto-plastic

Correspondence to: J. Bleyer, Laboratoire Navier, 6-8 av Blaise Pascal, Cité Descartes, 77455 Champs-sur-Marne, France, Tel : +33 (0)1 64 15 36 59

Email address: jeremy.bleyer@enpc.fr (Jeremy Bleyer)

URL: https://sites.google.com/site/bleyerjeremy/ (Jeremy Bleyer)

analyses of frame structures (e.g. step-by-step non-holonomic analyses, single step holonomic, hardening, softening...) in [9, 21, 39] and references cited therein.
Recent advances in mathematical programming have extended interior point algorithms to second-order cone programming (SOCP) problems [2, 15, 19, 20]. SOCP encompasses a larger class of convex optimization problems and an important number of the usual strength criteria can be formulated using SOCP constraints [5, 22], allowing us to obtain numerical estimates of limit loads with higher accuracy and small computation times. For these reasons, limit analysis using SOCP formulations has gained increasing attention and was successfully applied to 2D plane strain or plane stress problems [8, 23, 24, 27] as well as plates in bending problems [6, 17, 18].

In the case of yield design of frame structures made of composite sections, two approaches can be considered. First, one can treat the beam element as a 3D continuum and formulate the local yield criterion in terms of three-dimensional stress states. This was done in [16, 30] for reinforced concrete (RC) beams using a discrete zone model to define the internal stress state in the beam element. Obviously, the main drawback of this method is that it requires the construction of three-dimensional fields for which yield criteria have to be checked locally at an important number of points of the cross-section. It is, therefore, restricted to simple section geometries and reinforcement layouts.
The second approach formulates the section yield criterion in terms of generalized stresses such as axial forces, bending moments... According to this method, the frame members are considered as one-dimensional beam elements and equilibrium equations are written in terms of generalized stresses. This method is, therefore, particularly attractive from an engineering point of view, provided that the yield surface can be easily constructed. This approach has, notably, been used in plastic hinge yielding models for steel or composite frame structures [14, 42].
Early works considered linear programming to produce collapse mechanisms and related limit loads of frames with a yield criterion formulated on bending moments only [12, 28, 41]. In the early 80's, Nguyen-Dang Hung et al. [29] developed a computer software (CEPAO) to treat limit analysis with proportional loading and shakedown analysis with repeated cyclic loading on 2D frames, by linearizing the $N - M$ interaction yield surface. The method was extended in [13] to 3D steel frames using a 16-facet yield surface combining axial force and bending moments interaction. Piecewise linearization of the yield surface was also used in [25] for shakedown analysis on RC frames and in [4] for shakedown with parametrized load domains.
Computing accurate yield surfaces in combined axial force and bending moments has received increased attention in the literature [7, 11, 32, 34]. Convex nonlinear yield

surfaces are obtained for general composite sections and a convenient approximate representation is thus required to formulate an optimization problem. Piecewise linearization often requires an important number of polyhedral facets to obtain a sufficiently accurate approximation, which can have an important effect on the quality of the estimated bounds [31]. Since the yield criterion has to be verified for a large number of points throughout the whole structure, one often has to find a compromise between accuracy and computation time for large-scale problems.

To the authors' knowledge, the only attempt at treating limit and shakedown analysis of general composite frames under nonlinear yield surfaces was suggested by Skordeli and Bisbos [35]. In this work, steel frame yield surfaces were approximated by inner and outer ellipsoids so that the arising optimization problem became a SOCP problem. The global limit analysis problems with approximate yield surfaces were successfully solved by MOSEK [26], the standard industrial software package for large-scale and sparse SOCP problems. Results obtained in this paper seemed very promising and motivated our present work.
The novelty of this paper is to propose an accurate approximation procedure using more complex primitives than planes (piecewise linearization) or than one single ellipsoid (Skordeli and Bisbos [35]). The crucial part of the procedure is that only a few primitives will be needed to obtain a good approximation and to reduce the number of constraints for each criterion checking. In this paper, we propose an approximation using a sum of ellipsoids. This particular choice has two important advantages : first, formulating the yield surface as a sum of ellipsoids permits a simple analytical expression of the criteria in both primal and dual spaces; secondly, if the original yield surface is replaced by a sum of ellipsoids, the optimization problems arising in the static and kinematic limit analysis approaches both reduce to SOCP problems. As a result, a description of the yield surfaces using few parameters combined to the efficiency of SOCP solvers overcome the previously mentioned difficulty of the piecewise linearization approach and will allow to compute limit loads on complex structures with very low computational times.
First, we derive a dual description of general yield surfaces of composite sections (section 2). The approximation procedure will be detailed in section 3. The finite element method will be used in section 4 and 5 to formulate the static and kinematic approaches with the approximate yield surfaces as SOCP problems. Finally, the efficiency of the proposed method will be illustrated in section 6.

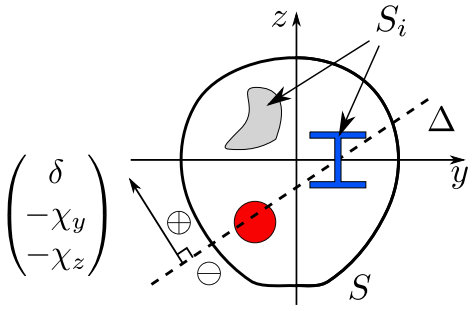

Figure 1: Composite beam section with different regions S_i associated to a local yield criterion $\mathcal{G}_i$

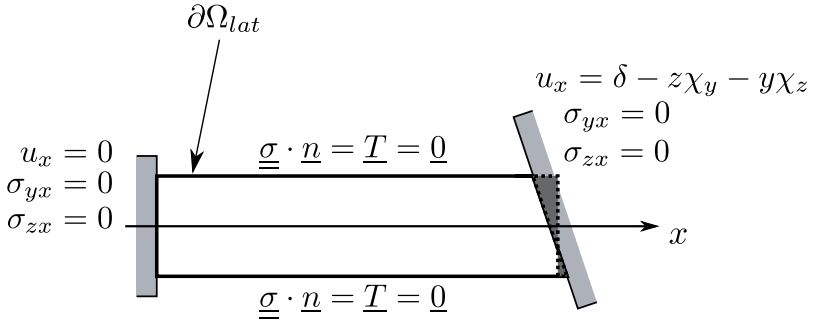

Figure 2: Auxiliary yield design problem

2. Combined biaxial bending interaction surface

Consider a beam oriented along direction x and of section S in the transverse (y, z) plane. Section S is made of different subsections S_i representing different materials and, in each S_i, the local yield criterion is defined through the corresponding domain $\mathcal{G}_i$ in the stress space (see figure 1). Perfect bonding is assumed between the subsections S_i.
Let σ_t^i (resp. σ_c^i) denote the ultimate strength in tension (resp. in compression) associated with yield criterion $\mathcal{G}_i$, defined by :

$$\sigma_t^i = \max\{\sigma \mid \sigma \underline{e}_x \otimes \underline{e}_x \in \mathcal{G}_i\}$$
$$\sigma_c^i = |\min\{\sigma \mid \sigma \underline{e}_x \otimes \underline{e}_x \in \mathcal{G}_i\}|$$

2.1. Auxiliary yield design problem

Our study is restricted to frame members infinitely resistant with respect to shear effects as well as torsion. Hence, yield surfaces will be drawn in the 3D space

involving axial force N and bending moments M_y and M_z. In order to compute such a generalized yield surface, the following auxiliary yield design problem is defined on a representative segment of length L of the composite beam (figure 2) :

- smooth contact with a fixed vertical plane at $x = 0$

$$u_x(x = 0, y, z) = 0 \tag{1}$$

$$\sigma_{xy}(x = 0, y, z) = \sigma_{xz}(x = 0, y, z) = 0 \tag{2}$$

- smooth contact with a plane rotating about $\Delta = \{(y, z) \mid \delta - z\chi_y - y\chi_z = 0\}$ at $x = L$

$$u_x(x = L, y, z) = \delta - z\chi_y - y\chi_z \tag{3}$$

$$\sigma_{xy}(x = L, y, z) = \sigma_{xz}(x = L, y, z) = 0 \tag{4}$$

- lateral boundary $\partial\Omega_{lat}$ is stress free

$$\underline{\underline{\sigma}} \cdot \underline{n} = \underline{0} \text{ on } \partial\Omega_{lat} \tag{5}$$

- external body forces are zero

(δ, χ_y, χ_z) may be interpreted as the generalized kinematic variables associated by duality to the generalized stress variables (N, M_y, M_z). Indeed, one can write, for all virtual velocity field $\underline{\widehat{u}}$ kinematically admissible (i.e. satisfying (1) and (3)), the virtual work of external loads as :

$$P_{ext}(\underline{\widehat{u}}) = \int_{\partial\Omega} \underline{n} \cdot \underline{\underline{\sigma}} \cdot \underline{\widehat{u}}\, dS$$

which yields using (1) to (5) :

$$P_{ext}(\underline{\widehat{u}}) = \delta \left(\int_{S(x=L)} \sigma_{xx} dS \right) + \chi_y \left(- \int_{S(x=L)} z\sigma_{xx} dS \right) + \chi_z \left(- \int_{S(x=L)} y\sigma_{xx} dS \right)$$

Now, defining the axial force and bending moments as the following stress resultants :

$$N = \int_{S(x=L)} \sigma_{xx} dS$$

$$M_y = - \int_{S(x=L)} z\sigma_{xx} dS$$

$$M_z = - \int_{S(x=L)} y\sigma_{xx} dS$$

the generalized strain and stress variables are, then, said to be in duality in the following sense :

$$P_{ext}(\widehat{\underline{u}}) = \delta N + \chi_y M_y + \chi_z M_z$$

which corresponds to a 3 parameters loading mode.

2.2. Computation of the generalized yield surface

In the following, it will be assumed that the generalized yield surface is conveniently described from using the following uniaxial stress fields :

$$\underline{\underline{\sigma}} = \begin{cases} \sigma_t^i \, \underline{e}_x \otimes \underline{e}_x & \text{if } \delta - z\chi_y - y\chi_z > 0 \text{ and } (y,z) \in S_i \\ -\sigma_c^i \, \underline{e}_x \otimes \underline{e}_x & \text{if } \delta - z\chi_y - y\chi_z < 0 \text{ and } (y,z) \in S_i \end{cases}$$

With $S_i^+ = S_i \cap \{\delta - z\chi_y - y\chi_z > 0\}$ and $S_i^- = S_i \cap \{\delta - z\chi_y - y\chi_z < 0\}$, we introduce the following definition :

$$(N, M_y, M_z) \in \mathcal{G}_u \Longleftrightarrow \exists(\delta, \chi_y, \chi_z) \left| \begin{array}{l} N = \displaystyle\sum_i \left(\int_{S_i^+} \sigma_t^i dS - \int_{S_i^-} \sigma_c^i dS \right) \\ M_y = \displaystyle\sum_i \left(\int_{S_i^-} z\sigma_c^i dS - \int_{S_i^+} z\sigma_t^i dS \right) \\ M_y = \displaystyle\sum_i \left(\int_{S_i^-} y\sigma_c^i dS - \int_{S_i^+} y\sigma_t^i dS \right) \end{array} \right. \tag{6}$$

This definition states that $\mathcal{G}_u$ is obtained by considering uniaxial stress fields reaching their maximum strength capacity in each region, either in tension or in compression, for different positions of the neutral axis Δ. Actually, we can only say that $\mathcal{G}_u$ is a lower bound estimate of the true yield surface $\mathcal{G} \supset \mathcal{G}_u$, but many design codes consider $\mathcal{G}_u$ as the true yield surface. The same assumption will be made in the following.

2.3. Dual formulation

The support function of $\mathcal{G}_u$ is defined by :

$$\pi(\delta, \chi_y, \chi_z) = \sup_{(N,M_y,M_z)\in\mathcal{G}_u} \{\delta N + \chi_y M_y + \chi_z M_z\}$$

or using (6),

$$\pi(\delta, \chi_y, \chi_z) = \sum_i \int_{S_i^+} \sigma_t^i \left(\delta - z\chi_y - y\chi_z\right) dS + \int_{S_i^-} \sigma_c^i \left|\delta - z\chi_y - y\chi_z\right| dS$$

which can also be written as :

$$\pi(\delta, \chi_y, \chi_z) = \sum_i \left(\int_{S_i} \sup \left\{ \sigma_t^i \left(\delta - z\chi_y - y\chi_z \right) ; -\sigma_c^i (\delta - z\chi_y - y\chi_z) \right\} dS \right) \qquad (7)$$

This equation shows that for a fixed direction in the dual space of generalized strains (δ, χ_y, χ_z), the support function of $\mathcal{G}_u$ can be easily computed from a numerical integration based on a discretization of the composite beam section.

2.4. Remarks and example

Both direct (6) and dual formulations (7) both show that it is no easy task to obtain a simple relationship between N, M_y and M_z describing the $\mathcal{G}_u$ boundary, making its use as a yield surface in a global limit analysis problem, impossible.
To illustrate the previous remark, an L-shaped reinforced concrete beam section was considered (figure 3(a)). Its yield surface was numerically computed using the above procedure in the (n, m_y, m_z) non-dimensional space with $n = N/N_0$, $m_y = M_y/M_{y0}$ and $m_z = M_z/M_{z0}$ where $\Sigma_0 = (|\min \Sigma| + \max \Sigma)/2$ for $\Sigma = N$, M_y or M_z. One can observe in figure 3(b) that the obtained interaction surface is of a quite complicated shape and, thus, cannot be correctly described by a simple analytical formula. A specific approximation procedure using numerical tools is thus required to obtain a simple description with few parameters.

3. Approximation of yield surfaces using a sum of ellipsoids

3.1. Illustrative example

Let us consider in this subsection the 2D yield surface of figure 4(a) representing a typical interaction curve between axial force N and bending moment M_y for a rectangular concrete section reinforced by one steel bar.
The traditional way of approximating such a yield surface is to use an inscribed or circumscribed polyhedron, as illustrated in figure 4(b) with $n = 16$ points. For yield surfaces in dimension 3 or even more, the required number of points to linearize a yield surface with a given accuracy becomes increasingly large. This is known as the "curse of dimensionality".
The Minkowski sum[1] of elementary objects (or primitives) allows us to represent convex sets with much fewer elements. For example, the unit cube in a d-dimensional space is made of 2^d vertices but can be described as the Minkowski sum of only d

[1]The Minkowski sum of two sets A and B is noted $A \oplus B$ and defined as $A \oplus B = \{c \mid \exists (a, b) \in A \times B \text{ such that } c = a + b\}$

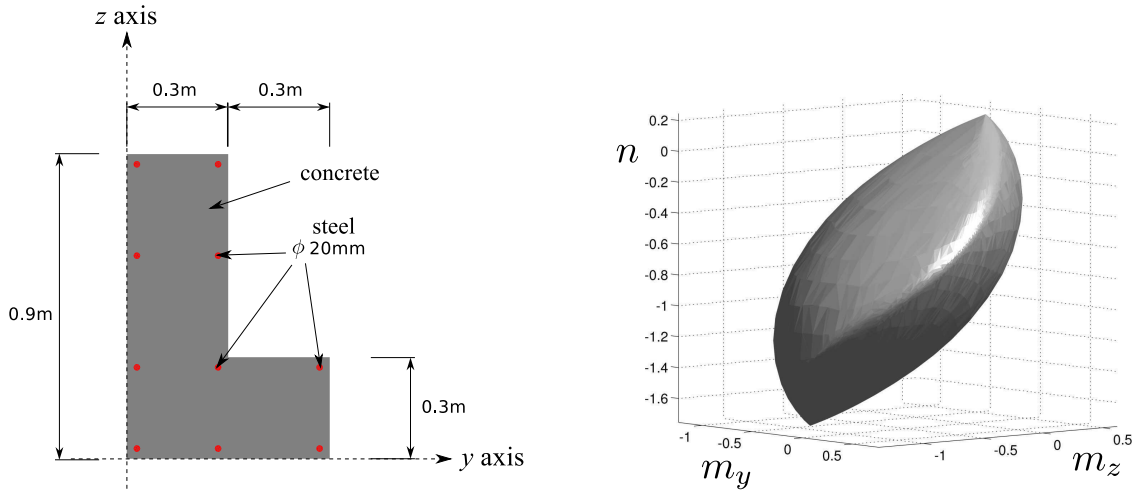

(a) Geometry (concrete in gray, steel reinforcements in red)

(b) Yield surface $\mathcal{G}_u$ in the (n, m_y, m_z) space

Figure 3: L-shaped reinforced concrete section. Considered strength values were $\sigma_c = 30$ MPa and $\sigma_t = 1.8$ MPa for concrete and $\sigma_c = \sigma_t = 435$ MPa for steel reinforcement.

unit segments along each direction.
Our idea is to use a Minkowski sum of ellipsoids to be more general than a sum of segments to approximate yield surfaces of beams, the main advantage being that the Minkowski sum of two ellipsoids does not produce an ellipsoid. In figure 5, we compared the convex set obtained by the Minkowski sum (in blue) of the two or three ellipses represented in black to the original interaction surface (in red). We can observe that with only three ellipses the quality of the approximation is as good as the one obtained with a $n = 16$ polytope.

3.2. Support function of a sum of ellipsoids

An ellipsoid $\mathcal{E}(Q, q)$ can be characterized by a symmetric positive semi-definite matrix Q defining its orientation and the length of its axis, and by a vector q collecting the coordinates of its center. Its support function can then be written as :

$$\pi_{\mathcal{E}}(d) = \sqrt{{}^T d \cdot Q \cdot d} + {}^T q \cdot d = \|C(Q) \cdot d\| + {}^T q \cdot d$$

where $C(Q)$ is the Cholesky factorization of matrix Q. Appendix A presents other useful relations between the ellipsoid equation and its support function.
A very interesting property of the Minkowski sum of two sets A and B is that the

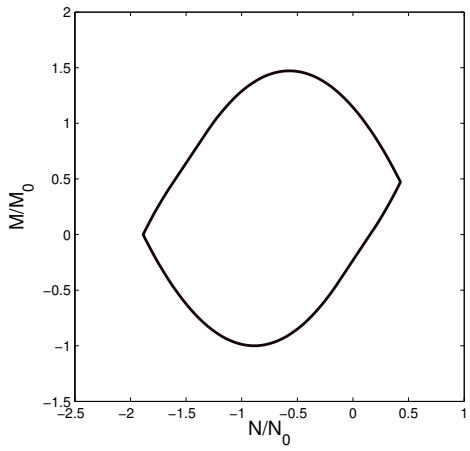

(a) Example of an interaction surface in 2D

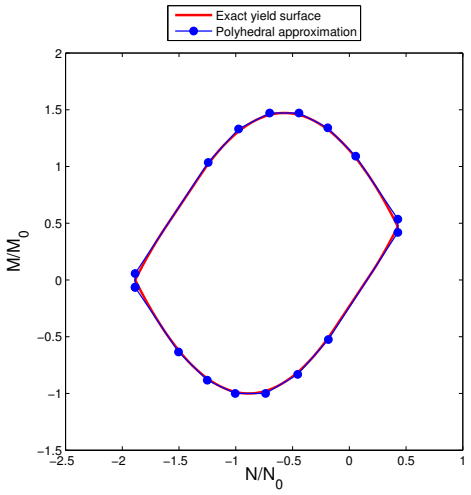

(b) Polyhedral approximation with 16 vertices

Figure 4: Illustrative example in 2D

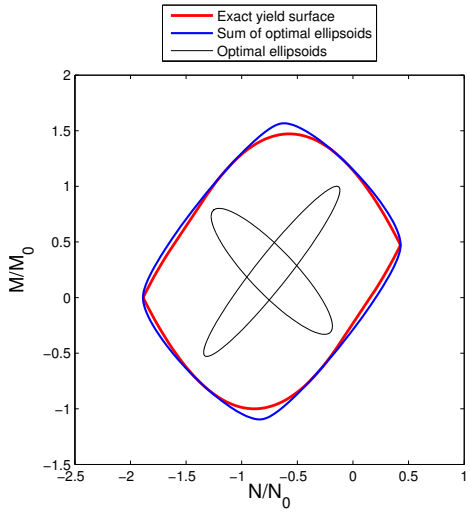

(a) $n_{ell} = 2$

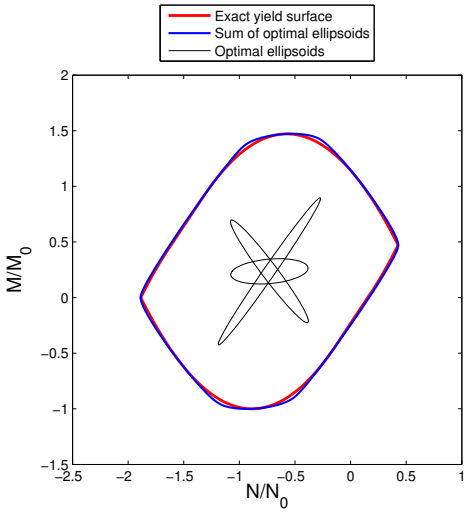

(b) $n_{ell} = 3$

Figure 5: Approximation of the interaction surface with n_{ell} ellipses

support function of $A \oplus B$ is equal to the sum of the support functions of A and of B. Hence, we will have for two ellipsoids $\mathcal{E}_1(Q_1, q_1)$ and $\mathcal{E}_2(Q_2, q_2)$ the following relation :

$$\pi_{\mathcal{E}_1 \oplus \mathcal{E}_2}(d) = \pi_{\mathcal{E}_1}(d) + \pi_{\mathcal{E}_2}(d) = \|C(Q_1) \cdot d\| + \|C(Q_2) \cdot d\| + {}^T(q_1 + q_2) \cdot d$$

3.3. Approximation procedure

Our objective is to approximate $\mathcal{G}_u$ by a sum of n ellipsoids. This is equivalent to approximating its support function $\pi_{\mathcal{G}_u}$ by the support function π_n of a sum of n ellipsoids. Therefore, we look for $C(Q_i)$ for $i = 1, \ldots, n$ and q such that :

$$\pi_{\mathcal{G}_u}(d) \approx \pi_n(d) = \sum_{i=1}^{n} \|C(Q_i) \cdot d\| + {}^T q \cdot d \qquad \forall d = (\delta, \chi_y, \chi_z)$$

To solve this problem, we chose to minimize the gap between both support functions in the least square sense for M points d_j belonging to the unit sphere in $\mathbb{R}^3$. Support functions are, indeed, positively 1-homogeneous, so that we can restrain their values to the unit sphere. Considering the coefficients of $C(Q_i)$ and q as an unknown vector $x \in \mathbb{R}^{6n+3}$ such that :

$$C(Q_i) = \begin{bmatrix} x_{6i-5} & x_{6i-4} & x_{6i-3} \\ 0 & x_{6i-2} & x_{6i-1} \\ 0 & 0 & x_{6i} \end{bmatrix} \quad ; \quad q = \begin{Bmatrix} x_{6n+1} \\ x_{6n+2} \\ x_{6n+3} \end{Bmatrix}$$

the minimization problem reduces to :

$$\min_{x \in \mathbb{R}^{6n+3}} \sum_{j=1}^{M} \left(\pi_{\mathcal{G}_u}(d_j) - \sum_{i=1}^{n} ||C(Q_i) \cdot d_j|| - {}^T q \cdot d_j \right)^2 \tag{8}$$

This is a general nonlinear least-square problem which was solved with the nonlinear solver implemented in MATLAB using the sequential quadratic programming (SQP) algorithm.

Let us mention that, since such approximations will be used in lower (resp. upper) bound limit analysis problems, we are interested in obtaining inscribed (resp. circumscribed) approximations. Various strategies can be imagined to obtain such lower and upper bound approximations. The first one consists in adding to problem (8) a nonlinear constraint : $\pi_{\mathcal{G}_u}(d_j) - \pi_n(d_j) \geq 0$ (resp. ≤ 0) for all j. However, this strategy would require to solve two non-linear optimization problems. Numerical experiments tend to show that minimization problems for upper approximations

yielded better solutions in general. Hence, we propose to solve problem (8) only with the $\pi_{\mathcal{G}_u}(d_j) - \pi_n(d_j) \leq 0$ constraint and, thus, compute :

$$\frac{1}{\alpha_-} = \max_j \frac{\pi_n(d_j) - {}^T q \cdot d_j}{\pi_{\mathcal{G}_u}(d_j) - {}^T q \cdot d_j}$$

Then, it can easily be seen that we have for all j :

$$\pi_n^-(d_j) = \alpha_-(\pi_n(d_j) - {}^T q \cdot d_j) + {}^T q \cdot d_j \leq \pi_{\mathcal{G}_u}(d_j) \leq \pi_n(d_j)$$

π_n^- is then a lower approximation of $\pi_{\mathcal{G}_u}$ obtained from scaling π_n by a factor α_- with respect to the center q so that the furthest supporting plane of π_n from $\pi_{\mathcal{G}_u}$ corresponds now to a supporting plane tangent to $\pi_{\mathcal{G}_u}$.

3.4. Illustration

The preceding approximation procedure has been applied to the L-shape RC beam example of subsection 2.4. Minimization problem with $M = 10\,000$ points on the unit sphere were solved with the `fmincon` MATLAB function. Optimal sums of ellipsoids were obtained for different values of n. Computation times ranged between a few seconds for one ellipsoid to less than five minutes for 5 ellipsoids.
In order to evaluate the quality of the approximation, we considered the relative error defined for all j by

$$\epsilon(\pi_n)_j = \frac{|\pi_n(d_j) - \pi_{\mathcal{G}_u}(d_j)|}{\pi_{\mathcal{G}_u}(d_j) - {}^T q \cdot d_j}$$

and its associated L^2 and L^∞ norms :

$$\|\epsilon(\pi_n)\|_2 = \left(\frac{1}{M} \sum_{j=1}^{M} (\epsilon(\pi_n)_j)^2 \right)^{1/2} \qquad \|\epsilon(\pi_n)\|_\infty = \max_j \epsilon(\pi_n)_j$$

In table 1, values of the error norms were given for different numbers of ellipsoids for both lower and upper approximations. We can see that with only a few ellipsoids ($n = 3$ for instance) the maximal error made on the exact criterion is less than 10% which is quite satisfactory.

The outer approximate yield surface obtained with 3 ellipsoids was represented in figure 6(a) in comparison to the exact one (in gray). A polyhedral outer approximation with 192 vertices was also represented in figure 7(a) to underline the difference of efficiency between the polyhedral approximation and the proposed method. Relative errors on the support functions for both methods were also plotted on the unit

n	$\|\epsilon(\pi_n^-)\|_2$ (%)	$\|\epsilon(\pi_n^-)\|_\infty$ (%)	$\|\epsilon(\pi_n))\|_2$ (%)	$\|\epsilon(\pi_n)\|_\infty$ (%)
1	16	17	6.4	23
2	11	12	2.9	14
3	8.6	9.5	1.9	10
5	5.4	6.6	1.1	7.3

Table 1: Norms of the relative errors for the different approximations

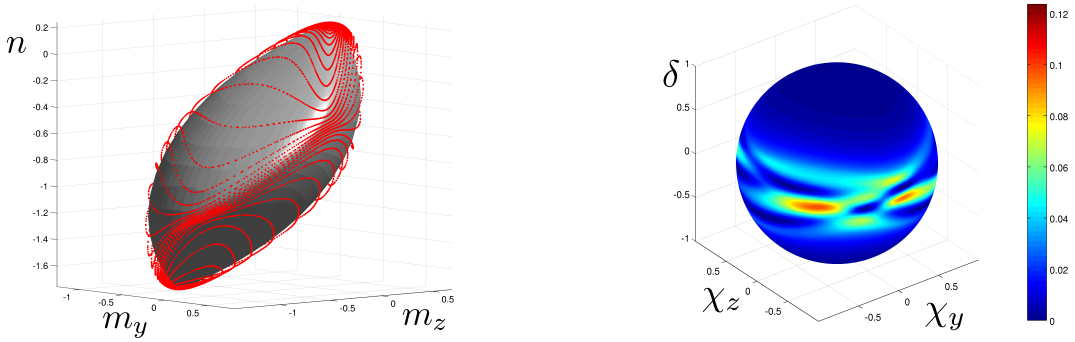

(a) 3D representation of outer approximation (red dots)

(b) Map of the relative error $\epsilon(\pi_3)$ on the unit sphere

Figure 6: Approximation with 3 ellipsoids

sphere in the dual space of generalized strains in figure 6(b) and 7(b). The maximal error for the polyhedral approximation is about 12% and the mean squared error is 3.2% which shows that the proposed method gives better results with 3 ellipsoids than a polytope with 192 vertices.

Intersections with different planes $m_z = cst$ were plotted in figure 8 for outer and inner approximations with 3 ellipsoids. Even if inner approximations are of lesser quality than outer approximations with the retained strategy, their precision is still acceptable for their use in limit analysis.

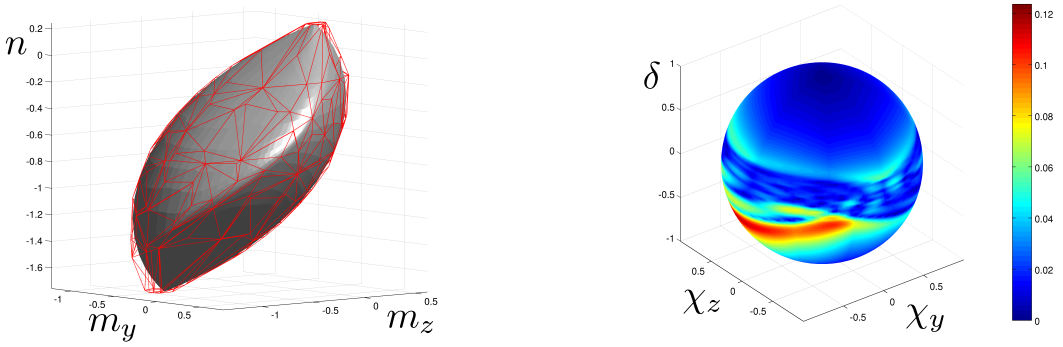

(a) 3D representation of outer approximation (red lines)

(b) Map of the relative error on the unit sphere

Figure 7: Approximation using a polytope with 192 vertices

4. Numerical formulation of the kinematic approach for the global structure

4.1. Finite element discretization

The global structure is discretized using 3D beam elements with 2 nodes and 6 degrees of freedom (dof) per node [3] : axial displacement of the beam u along x, transversal displacements v and w in directions y and z and rotations around each axis : θ_x, θ_y and θ_z (see figure 9). The Euler-Bernoulli conditions can be written as :

$$\theta_y = \frac{dw}{dx} \quad \text{and} \quad \theta_z = \frac{dv}{dx}$$

and curvatures are thus given by :

$$\chi_y = \frac{d^2w}{dx^2} \quad \text{et} \quad \chi_z = \frac{d^2v}{dx^2}$$

while we have $\delta = \dfrac{du}{dx}$ for axial extension and $\omega = \dfrac{d\theta_x}{dx}$ for torsion strain. The expression of the finite element strain matrix are given in appendix Appendix B.

Assuming that in each point, the local yield criterion has been approximated by a sum of n ellipsoids (with J_i matrices and center vector q obtained from the outer approximation procedure of section 3.3), we introduce the support function of the yield criterion where torsion has been penalized :

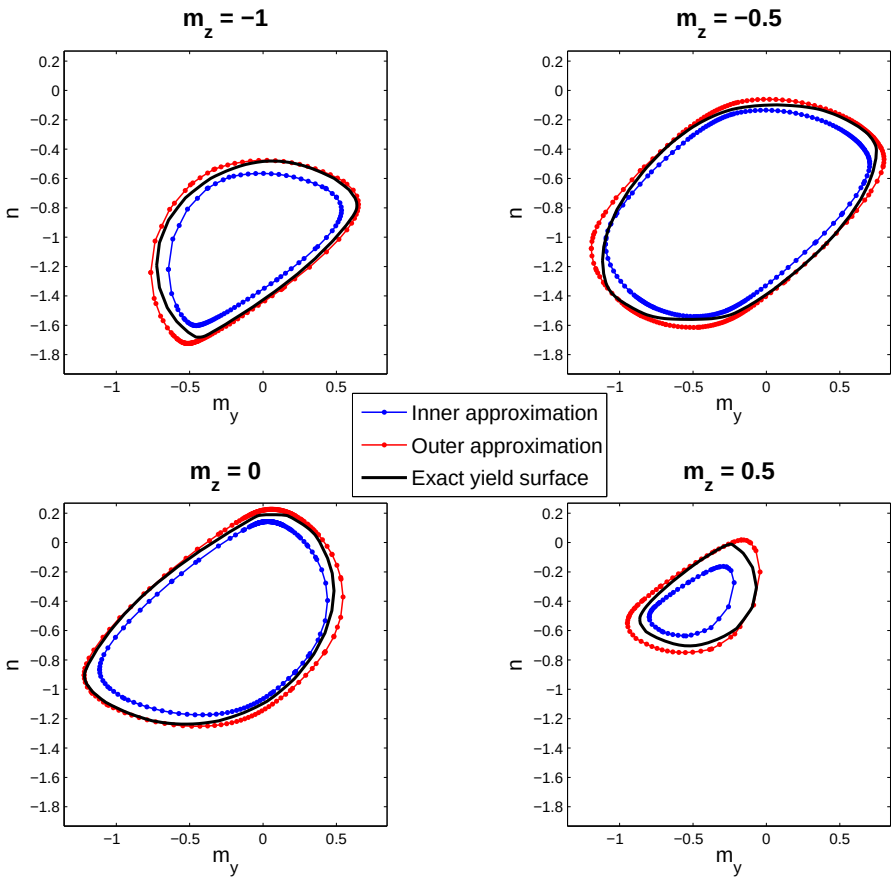

Figure 8: Intersections of approximate and exact yield surfaces with different planes $m_z = cst$

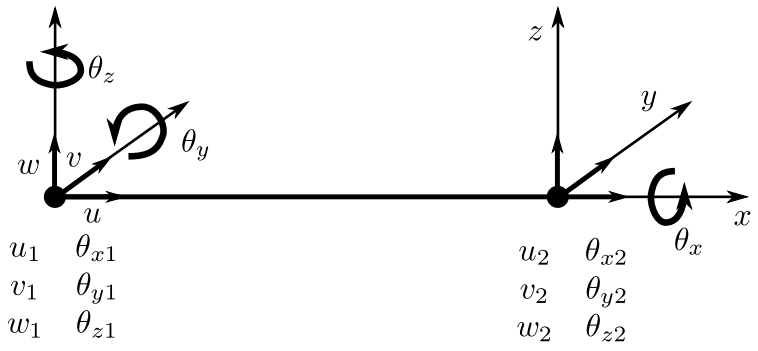

Figure 9: Displacement finite element

$$\pi(\delta, \chi_y, \chi_z, \omega) = \sum_{i=1}^{n} \left\| \widetilde{J}_i \cdot d \right\| + {}^T\widetilde{q} \cdot d$$

$$\text{where } \widetilde{J}_i = \left[\begin{array}{ccc|c} & J_i & & \begin{matrix}0\\0\\0\end{matrix} \\ \hline 0 & 0 & 0 & T_{pen} \end{array}\right], \quad \widetilde{q} = \left\{\begin{matrix} q \\ \\ 0 \end{matrix}\right\} \quad \text{and} \quad d = \left\{\begin{matrix} \delta \\ \chi_y \\ \chi_z \\ \omega \end{matrix}\right\} \tag{9}$$

where T_{pen} is a penalization term equal to $10^2 \cdot \max J_i$. It is worth noting that such a yield criterion is now written in the 4-dimensional space including torsion and that it is very easy to add a torsion term in the particular form of the ellipsoidal approximation.

4.2. Upper bound limit analysis problem

We assume that the external loads can be decomposed as $\lambda F + F_0$ where F_0 represents a dead load and λF is the multiplicative load for which we are interested in finding the limit value at collapse through the multiplier λ. Hence, in a given kinematically admissible displacement field U, the power of external loads is $P_{ext}(U) = \lambda^T F \cdot U + {}^T F_0 \cdot U$.

The maximum resisting work is given by the integral of the local support function on the whole structure Ω :

$$P_{rm}(U) = \int_{\Omega} \pi(d[U]; x) d\Omega$$

where $d[U]$ is the strain vector related to U at point x.

The upper bound limit analysis problem consists in solving the following minimization problem :

$$\lambda_{UB} = \min_{^TF \cdot U = 1} \left(P_{rm}(U) - {}^T F_0 \cdot U \right)$$

4.3. Formulation as a standard SOCP problem

For the sake of notation simplicity, we will consider that the local yield criterion is the same for each point of the structure and can be written in the form of equation (9). Obviously, generalization to a structure made of different types of beam sections will only have to consider different parameters J_i and q at each finite element e and varying values of n with e.

Due to the non-linearity of the local support functions, integration at the element level has to be performed using a Gaussian quadrature rule with m points $\xi_g \in [-1; 1]$ for $g = 1, ..., m$. Thus, letting $R_{i,g,e} = \widetilde{J}_i \cdot B_e(\xi_g)$ we have :

$$P_{rm} = \sum_{e=1}^{N_e} \sum_{g=1}^{m} c_{e,g} \left(\sum_{i=1}^{n} \| R_{i,g,e} \cdot U_e \| + {}^T\widetilde{q} \cdot B_e(\xi_g) \cdot U_e \right)$$

where $c_{e,g}$ are weighting coefficients coming from the quadrature rule. Finally, introducing auxiliary variables $r_{i,g,e} = R_{i,g,e} \cdot U_e$ and $t_{i,g,e} = \| r_{i,g,e} \|$, we obtain the following discrete minimization problem :

$$\begin{aligned} \lambda_{UB} = \quad & \min \sum_{e=1}^{N_e} \sum_{g=1}^{m} c_{e,g} \left(\sum_{i=1}^{n} t_{i,g,e} + {}^T\widetilde{q} \cdot B_e(\xi_g) \cdot U_e \right) - {}^T F_0 \cdot U \\ & {}^T F \cdot U = 1 \\ & r_{i,g,e} = R_{i,g,e} \cdot U_e \\ & t_{i,g,e} \geq \| r_{i,g,e} \| \qquad \forall i, e, g = 1, ..., n \cdot m \cdot N_e \end{aligned} \tag{10}$$

Problem (10) consists in the minimization of a linear function of U under $1+4n \cdot m \cdot N_e$ linear equality constraints and $n \cdot m \cdot N_e$ quadratic cone constraints which is the standard formulation of an SOCP problem.

4.4. Remarks

If piecewise linearization of the yield surface with p vertices had been chosen, support functions would be expressed as a maximum of p linear functions of U at each integration point. This would lead to a LP problem involving $p \cdot m \cdot N_e$ linear inequality constraints.
For example, considering a structure made of $N_e = 500$ elements, using a $m = 3$

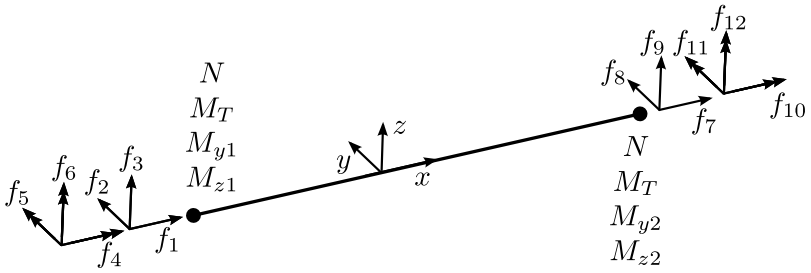

Figure 10: Equilibrium finite element

points quadrature rule, the ellipsoidal approximation with $n = 3$ ellipsoids would produce 18 000 linear equality constraints and 4 500 conic constraints. On the other hand, for the same problem, a polyhedral approximation with $p = 192$ vertices would produce 288 000 linear inequality constraints...

5. Numerical formulation of the static approach for the global structure

5.1. Equilibrium finite element

In order to solve a lower bound limit analysis problem, the structure is discretized into finite elements on which local equilibrium equations are verified. We chose a classical two noded element with linear distribution of the bending moments M_y and M_z, the constant normal force N, and the torsional moment M_T. More details can be found in [10, 40]. Local equilibrium between the 6 nodal stress variables ${}^T\Sigma_e = (N, M_T, M_{y1}, M_{z1}, M_{y2}, M_{z2})$ and nodal forces and moments of the beam element $f_e = (f_{e,j})_{j=1,\dots,12}$ (figure 10) is expressed through an elementary equilibrium matrix h_e such that $f_e = h_e \cdot \Sigma_e$. Global equilibrium is then obtained after assembling elemental contributions in a global matrix H such that we have :

$$H \cdot \Sigma = \lambda F + F_0$$

where Σ is the global vector of stress parameters. We note that H is a $N_q \times 6N_e$ matrix where N_q is the number of equilibrium equations after taking boundary conditions into account.

5.2. Global yield criterion constraints

In the following, we will assume that, for a given finite element e, the local yield criterion expressed in terms of generalized variables ${}^T\sigma = (N, M_y, M_z, M_T) \in \mathbb{R}^4$ can

be written as a sum of ellipsoids of the following type :

$$\sigma \in \mathcal{G} = \bigoplus_{i=1}^{n} \widetilde{\mathcal{E}}_i(J_i, 0) \oplus q \tag{11}$$

where parameters J_i and q are given by the approximation procedure described in the previous section and include the same penalization term for torsion as for the kinematic approach. Equation (11) can also be expressed as :

$$\sigma \in \mathcal{G} \Longleftrightarrow \exists\, \sigma_1, \ldots, \sigma_n \text{ s.t. } \begin{cases} \sigma = \sigma_1 + \ldots + \sigma_n + q \\ \sigma_i \in \widetilde{\mathcal{E}}_i(J_i, 0) \quad \forall i = 1, \ldots, n \end{cases}$$

Or, equivalently :

$$\sigma \in \mathcal{G} \Longleftrightarrow \exists\, \tau_1, \ldots, \tau_n \text{ s.t. } \begin{cases} \sigma = {}^T J_1 \cdot \tau_1 + \ldots + {}^T J_n \cdot \tau_n + q \\ ||\tau_i|| \leq 1 \quad \forall i = 1, \ldots, n \end{cases} \tag{12}$$

which is a standard form of SOCP constraints involving auxiliary variables τ_i.

We also note that, due to the choice of linear (or constant) interpolation of stress parameters over an element and the convexity of the yield surface, the yield criterion has only to be checked at the nodes of a given element e. Hence, constraint (12) will be enforced for ${}^T\sigma_{e1} = (N, M_{y1}, M_{z1}, M_T)$ and for ${}^T\sigma_{e2} = (N, M_{y2}, M_{z2}, M_T)$.

Finally, the discretized static approach leads to the following maximization problem :

$$\begin{aligned} \lambda_{LB} = \quad & \max \lambda \\ & H \cdot \Sigma = \lambda F + F_0 \\ & \Sigma = {}^T J \cdot \tau + Q \\ & \|\tau_{i,e}\| \leq 1 \quad \forall i, e = 1, ..., 2n \cdot N_e \end{aligned} \tag{13}$$

where the last two constraints express the global form of constraint (12). Problem (13) reduces to the maximization of a single variable λ under $N_q + (8 + 2n) \cdot N_e$ linear equality constraints and $2n \cdot N_e$ quadratic cone constraints which is the standard formulation of a SOCP problem.

6. Illustrative application

The purpose of this section is to illustrate the performance of the proposed method on a complex frame structure. Figure 11 represents the isometric view of

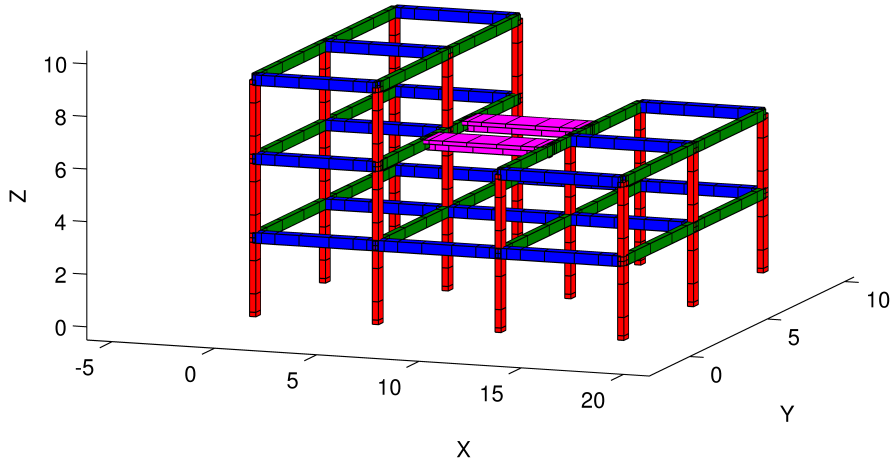

Figure 11: 3D view of the considered structure (section a in blue, section b in green, section c in red and section d in magenta)

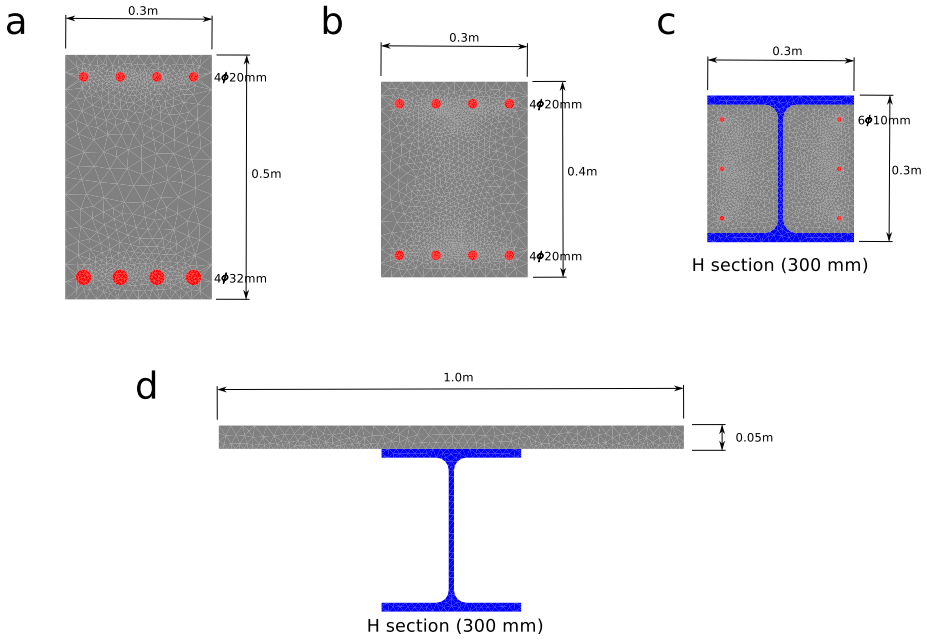

Figure 12: Geometry of the different sections : principal beams (section a), secondary beams (section b), columns (section c) and footbridge (section d). Materials : concrete in gray ($\sigma_c = 30$ MPa, $\sigma_t = 1.8$ MPa), construction steel in blue and reinforcement bars in red ($\sigma_c = \sigma_t = 435$ MPa)

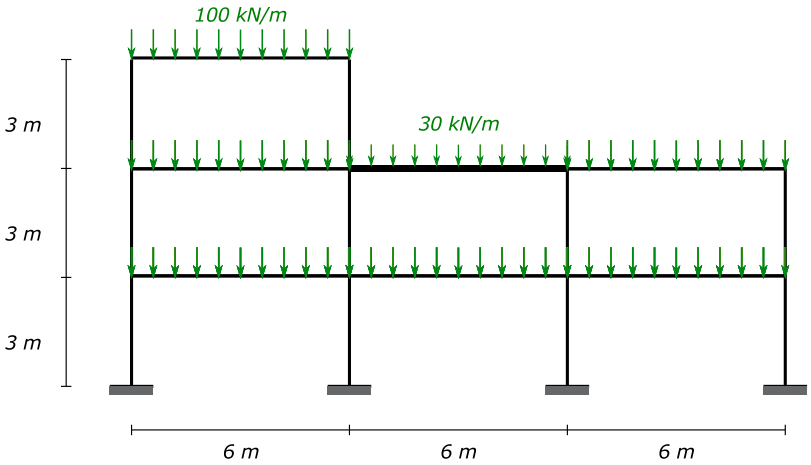

(a) Elevation view of the structure and considered dead loads

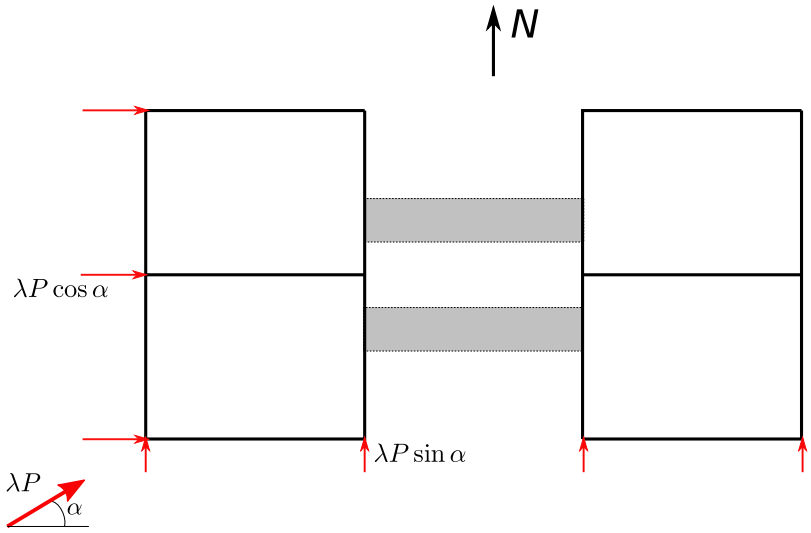

(b) Plane view of the structure and considered wind loading

Figure 13: Elevation and plane views

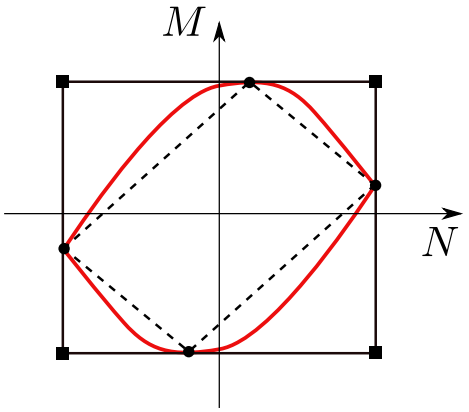

Figure 14: Piecewise linear approximations in a 2D space : inscribed approximation connecting ultimate axial force and bending capacities (dashed black line) and circumscribed approximation tangent to ultimate capacities (solid black line)

a 3-storey building frame consisting of four different structural groups : principal beams (represented in blue), secondary beams (represented in green), columns (represented in red) and two footbridges (represented in magenta). Members of the same structural group have the same section which are represented in figure 12. Principal and secondary beams are reinforced concrete sections, columns are steel H-section filled with concrete whereas footbridges' section consists of a RC slab supported by a steel H-section.
Uniform loading of intensity $g_1 = 100$ kN/m on every principal beams and $g_2 = 30$ kN/m on both footbridges corresponds to a dead load (weight), collected in F_0 (figure 13(a)). Wind loading is modeled via nodal forces applied to beam-column connections on West, South and East sides of the building (figure 13(b)). Considering a force of intensity λP making an angle α with the $X-$axis :

- nodal forces on West side will be $\lambda P \cos\alpha \underline{e}_X$ if $0° \leq \alpha \leq 90°$ and 0 otherwise
- nodal forces on East side will be $\lambda P \cos\alpha \underline{e}_X$ if $90° \leq \alpha \leq 180°$ and 0 otherwise
- nodal forces on South side will be $\lambda P \sin\alpha \underline{e}_Y$ for $0° \leq \alpha \leq 180°$

The frame was discretized using 10 elements for each principal beam and footbridge, 8 elements for each secondary beam and 6 elements for each column, making a total of 540 elements. The element size was refined near beam-column connections and $m = 3$ Gauss points were used for the upper bound kinematic approach.

The approximation procedure described in section 3.3 was performed on the 4 different section types. Yield surfaces were approximated using $n = 3$ ellipsoids and maximal relative errors for inner and outer approximation are given in table 2. The optimization step took around 4 minutes in each case to find the optimal ellipsoids. The lower bound and upper bound SOCP problems (10) and (13) were solved using the previously mentioned MOSEK software package.
The problem was also analyzed using a piecewise-linear inscribed approximation by a polytope with $p = 6$ vertices (corresponding to ultimate normal force and bending moment capacities) and a piecewise-linear circumscribed approximation using a box-shaped polytope with $p = 8$ vertices (whose facets are tangent to the ultimate normal force and bending moment capacities). An illustration in a 2D case is represented in figure 14. The corresponding optimization problems were formulated as standard linear programming (LP) problems and also solved using MOSEK.

Limit loads were computed for 40 different values of wind incidence α using the lower bound static approach combined with inscribed approximations and the upper bound kinematic approach combined with circumscribed approximations. Values of the obtained limit load estimates are represented in figure 15. First, one can observe that static approaches with inscribed approximations produce lower estimates than kinematic approaches with circumscribed approximations. As expected, ellipsoidal approximations produce closer bounds than the considered polyhedral approximations. With the ellipsoidal approximation technique, one can expect to bracket the limit load with $\pm 8\%$ relative accuracy (as an average on all load cases) whereas with the polyhedral approximation only $\pm 30\%$ can be expected. It is also worth noting that, for a given load case, the global optimization step took, as an average, 3.8 s for the polyhedral lower bound, 3.4 s for the polyhedral upper bound, 1.8 s for the ellipsoidal lower bound and 2.6 s for the ellipsoidal upper bound. Thus, despite the small number of vertices for the polyhedral approximations and the fact that SOCP problems are expected to be more difficult to solve than LP problems, the ellipsoidal approximation technique seems highly advantageous in terms of computing time as well as accuracy.

Obviously, when considering computational costs, one has also to consider the cost of the approximation procedure for finding the optimal ellipsoidal approximation. In the case of a structure consisting of an important number of section geometries, this step can represent a non-negligible aspect of the computing time. Nevertheless, it is important to keep in mind that it is only a preprocessing step. Indeed, since only a few parameters are required to describe the yield surface, these can easily be

Section type	Inscribed	Circumscribed
Principal beam	11.0%	12.3%
Secondary beam	12.0%	13.7%
Column	11.4%	12.9%
Footbridge	8.2%	8.9%

Table 2: Maximal relative errors (in %) made with $n = 3$ ellipsoids for the different section types

saved once and for all for a given geometry section. Moreover, one difficult aspect of non-linear structural analysis is that different load cases cannot be combined using the superposition principle as in linear elastic analysis. Engineers are thus often constrained to consider a limited number of loading cases for non-linear analysis. With such direct methods as limit analysis, one can easily compute an important number of different loading cases, once the yield surfaces have been determined.

7. Extension of the approximation procedure for other types of yield surfaces

In this work, we proposed to approximate the considered convex yield surfaces by a Minkowski sum of ellipsoids. Unfortunately, this method cannot be applied to all convex sets. Mathematical results on convex geometry show that a sum of ellipsoids is not dense in the set of convex sets.
In this work, the considered yield surfaces represent a particular class of convex sets called "zonoids". A zonoid is a convex body which can be approximated by a finite sum of segments. Expression (7) shows that $\mathcal{G}_u$ is, indeed, a zonoid since the integrand at a point (y, z) on the section S corresponds to the support function of a segment. Hence, the support function can be approximated with an arbitrary precision by a finite sum of support functions of segments (by simply performing a quadrature of the integral). Since a sum of segments is a special case of a sum of ellipsoids, the considered yield surfaces in this work can be approximated by a finite sum of ellipsoids. However, this is only due to the fact that we considered only uniaxial strength of the local material.
Therefore, yield surfaces are not zonoids in general and the presented approximation method will inevitably fail in other cases. Nevertheless, we would like to underline that the main idea of this work is to develop approximation procedures of convex yield surfaces so that they can be analytically described by a few parameters and so that corresponding optimization problems can be efficiently treated by a dedicated SOCP solver. Future work will, thus, consist in developing new approximation techniques

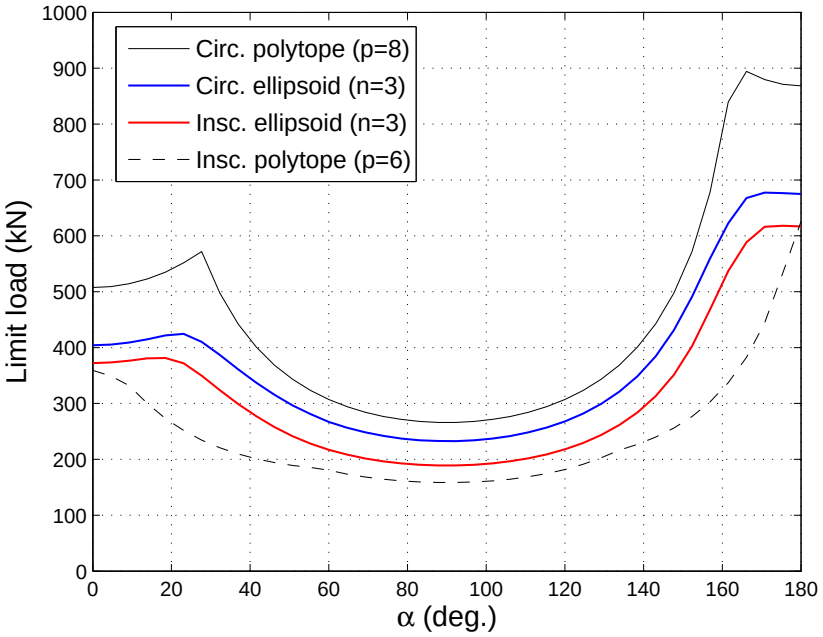

Figure 15: Limit loads obtained with different approximations

following these objectives. A current work is investigating the possibility of using a convex hull of ellipsoids for general convex yield surfaces approximation.

8. Conclusion

In the present work, the application of static and kinematic approaches of yield design theory to three-dimensional structures consisting of composite beam sections is investigated. Integration of the local material strength at the section level permits us to obtain a generalized yield surface characterizing the ultimate strength domain of the section in the space of axial force and bending moments. Computation of such yield surfaces on different types of composite sections shows that these convex bodies cannot be easily described and, therefore, cannot be injected into a mathematical optimization solver. To overcome such a difficulty, a classical approach is to linearize the considered yield surfaces from inside or from outside given the type of approach we want to conduct. However, a large number of planes is often required to perform such piecewise linearizations, introducing an important number of auxiliary variables in the optimization problem formulated at the structure level.

To improve computational efficiency, one can consider more complex geometric primitives for yield surface approximation. In the particular case of composite beams, we proposed to use a sum of ellipsoids, for which an analytical description is easily available. Moreover, this choice makes it possible to use efficient interior point algorithms to solve the associated SOCP problem for both static and kinematic approaches. An approximation procedure using the support function description and nonlinear optimization solvers was proposed to compute optimal ellipsoids. Numerical examples showed that very good accuracy can be obtained with only a few ellipsoids.

The proposed method was subsequently applied to a complex frame structure consisting of different types of composite sections. Both static and kinematic approaches were formulated using the finite element method and solved with the Mosek software. Limit loads were obtained within seconds on a personal computer which underlines the attractiveness of the method from an engineering point of view. Our work has only considered limit analysis of frames for the sake of simplicity, but it can be extended without any supplementary difficulty to shakedown analysis.

Despite the fact that a sum of ellipsoids can only be used in this particular case, this work shows that efficient approximation techniques can be combined with optimization solvers to tackle complex yield design problems. Extension of this approach to macroscopic yield surfaces, obtained via a homogenization procedure, will make it possible to compute limit loads of complex structures made of heterogeneous materials in the near future.

Appendix A. Ellipsoids and support function

Let us consider an ellipsoid $\mathcal{E}$ of half axis lengths a_1, a_2 and a_3 in the three orthogonal unit directions n_1, n_2 and n_3 and centered at a point q. Its equation reads :

$$\left(\frac{\Sigma_1 - q_1}{a_1}\right)^2 + \left(\frac{\Sigma_2 - q_2}{a_2}\right)^2 + \left(\frac{\Sigma_3 - q_3}{a_3}\right)^2 \leq 1$$

where $\Sigma_i = {}^T\Sigma \cdot n_i$ and $q_i = {}^T q \cdot n_i$. Hence, introducing the rotation matrix $R = {}^T[n_1\, n_2\, n_3]$ and $J = \text{diag}\,(a_1, a_2, a_3) \cdot R$, we also have :

$$\mathcal{E} = \left\{\Sigma \text{ s.t. } \left\|{}^T J^{-1} \cdot (\Sigma - q)\right\| \leq 1\right\} \tag{A.1}$$

Its support function can then be easily obtained :

$$\pi(D) = \sup_{\Sigma \in \mathcal{E}} {}^T\Sigma \cdot D = \sup_{\|\widetilde{\Sigma}\| \leq 1} {}^T\widetilde{\Sigma} \cdot J \cdot D + {}^T q \cdot D$$

$$\pi(D) = \|S \cdot D\| + {}^T q \cdot D = \sqrt{{}^T D \cdot Q \cdot D} + {}^T q \cdot D \tag{A.2}$$

with $Q = {}^T J \cdot J = {}^T R \cdot \text{diag}\,(a_1^2, a_2^2, a_3^2) \cdot R$. Let us remark that this expression is still valid even in the case when the ellipsoid degenerates (some $a_i = 0$). Hence, an ellipsoid can thus be characterized by a symmetric semi-definite positive matrix Q (or its Cholesky factorization $C(Q) = J$) along with a vector q.

Appendix B. Generalized strain matrix for a displacement finite element

The chosen displacement finite element uses the classical cubic Hermite interpolation for transversal displacements v and w. Interpolation of axial displacement u and rotation θ_x are both linear. Hence, for a given finite element of length l, the relations between the strain vector d and the 12 dof of a given element with endpoints

1 and 2 are given $\forall \xi = x/l \in [0;1]$ by :

$$\begin{aligned}
\delta(\xi) &= \begin{Bmatrix} -1/l & 1/l \end{Bmatrix} \begin{Bmatrix} u_1 \\ u_2 \end{Bmatrix} \\
\chi_y(\xi) &= \frac{1}{l^2} \begin{Bmatrix} 12\xi - 6 & 6\xi l - 4l & -12\xi + 6 & 6\xi l - 2l \end{Bmatrix} \begin{Bmatrix} w_1 \\ \theta_{z1} \\ w_2 \\ \theta_{z2} \end{Bmatrix} \\
\chi_z(\xi) &= \frac{1}{l^2} \begin{Bmatrix} 12\xi - 6 & 6\xi l - 4l & -12\xi + 6 & 6\xi l - 2l \end{Bmatrix} \begin{Bmatrix} v_1 \\ \theta_{y1} \\ v_2 \\ \theta_{y2} \end{Bmatrix} \\
\omega(\xi) &= \begin{Bmatrix} -1/l & 1/l \end{Bmatrix} \begin{Bmatrix} \theta_{x1} \\ \theta_{x2} \end{Bmatrix}
\end{aligned} \tag{B.1}$$

which can be condensed under the following form $d = b_e(\xi) \cdot u_e$ where u_e represents the 12 elemental dof vector expressed in the local axis of the current element. One still has to apply a rotation matrix to express generalized strains in terms of degrees of freedom expressed in the global axis of the structure $d = b_e(\xi) \cdot R_e \cdot U_e = B_e(\xi) \cdot U_e$.

References

[1] Anderheggen, E., Knöpfel, H.. Finite element limit analysis using linear programming. International Journal of Solids and Structures 1972;8(12):1413–1431.

[2] Andersen, K.D., Christiansen, E., Overton, M.L.. Computing limit loads by minimizing a sum of norms. SIAM Journal on Scientific Computing 1998;19(3):1046–1062.

[3] Batoz, J.L., Dhatt, G.. Modélisation des structures par éléments finis: Poutres et plaques. Modélisation des structures par éléments finis. Hermès, 1990.

[4] Bisbos, C.D., Ampatzis, A.T.. Shakedown analysis of spatial frames with parameterized load domain. Engineering Structures 2008;30(11):3119–3128.

[5] Bisbos, C.D., Pardalos, P.M.. Second-order cone and semidefinite representations of material failure criteria. Journal of Optimization Theory and Applications 2007;134(2):275–301.

[6] Bleyer, J., de Buhan, P.. On the performance of non-conforming finite elements for the upper bound limit analysis of plates. International Journal for Numerical Methods in Engineering 2013;94(3):308–330.

[7] Charalampakis, A.E., Koumousis, V.K.. Ultimate strength analysis of composite sections under biaxial bending and axial load. Advances in Engineering Software 2008;39(11):923–936.

[8] Ciria, H., Peraire, J., Bonet, J.. Mesh adaptive computation of upper and lower bounds in limit analysis. International journal for numerical methods in engineering 2008;75(8):899–944.

[9] Cohn, M.Z., Maier, G., Grierson, D.E.. Engineering Plasticity by Mathematical Programming: Proceedings of the NATO Advanced Study Institute, University of Waterloo, Waterloo, Canada, August 2-12, 1977. Pergamon Press, 1979.

[10] Damkilde, L., Krenk, S.. Limitsa system for limit state analysis and optimal material layout. Computers & structures 1997;64(1):709–718.

[11] De Vivo, L., Rosati, L.. Ultimate strength analysis of reinforced concrete sections subject to axial force and biaxial bending. Computer methods in applied mechanics and engineering 1998;166(3):261–287.

[12] Grierson, D.E., Gladwell, G.M.L.. Collapse load analysis using linear programming. Journal of the structural Division 1971;97(5):1561–1573.

[13] Hoang, V.L., Nguyen-Dang, H.. Limit and shakedown analysis of 3-d steel frames. Engineering Structures 2008;30(7):1895 – 1904.

[14] Iu, C.K., Bradford, M.A., Chen, W.F.. Second-order inelastic analysis of composite framed structures based on the refined plastic hinge method. Engineering Structures 2009;31(3):799–813.

[15] Krabbenhoft, K., Damkilde, L.. A general non-linear optimization algorithm for lower bound limit analysis. International Journal for Numerical Methods in Engineering 2003;56(2):165–184.

[16] Larsen, K., Poulsen, P., Nielsen, L.. Limit analysis of 3d reinforced concrete beam elements. Journal of Engineering Mechanics 2012;138(3):286–296.

[17] Le, C.V., Gilbert, M., Askes, H.. Limit analysis of plates using the efg method and second-order cone programming. International Journal for Numerical Methods in Engineering 2009;78(13):1532–1552.

[18] Le, C.V., Nguyen-Xuan, H., Nguyen-Dang, H.. Upper and lower bound limit analysis of plates using fem and second-order cone programming. Computers & Structures 2010;88(1-2):65–73.

[19] Lyamin, A.V., Sloan, S.W.. Lower bound limit analysis using non-linear programming. International Journal for Numerical Methods in Engineering 2002;55(5):573–611.

[20] Lyamin, A.V., Sloan, S.W.. Upper bound limit analysis using linear finite elements and non-linear programming. International Journal for Numerical and Analytical Methods in Geomechanics 2002;26(2):181–216.

[21] Maier, G.. Piecewise linearization of yield criteria in structural plasticity. Solid Mechanics Archives 1976;1:239–281.

[22] Makrodimopoulos, A.. Remarks on some properties of conic yield restrictions in limit analysis. International Journal for Numerical Methods in Biomedical Engineering 2010;26(11):1449–1461.

[23] Makrodimopoulos, A., Martin, C.M.. Lower bound limit analysis of cohesive-frictional materials using second-order cone programming. International Journal for Numerical Methods in Engineering 2006;66(4):604–634.

[24] Makrodimopoulos, A., Martin, C.M.. Upper bound limit analysis using simplex strain elements and second-order cone programming. International journal for numerical and analytical methods in geomechanics 2007;31(6):835–865.

[25] Malena, M., Casciaro, R.. Finite element shakedown analysis of reinforced concrete 3d frames. Computers & Structures 2008;86(11):1176–1188.

[26] Mosek, . The mosek optimization toolbox for matlab manual. 2008.

[27] Munoz, J.J., Bonet, J., Huerta, A., Peraire, J.. Upper and lower bounds in limit analysis: Adaptive meshing strategies and discontinuous loading. International Journal for Numerical Methods in Engineering 2009;77(4):471–501.

[28] Neal, B.G., Symonds, P.S.. The rapid calculation of the plastic collaps load for a framed structure. In: ICE Proceedings: Engineering Divisions. Ice Virtual Library; volume 1; 1952. p. 58–71.

[29] Nguyen-Dang, H.. Cepao - an automatic program for rigid-plastic and elastic-plastic analysis and optimization of frame structures. Engineering Structures 1984;6(1):33 – 51.

[30] Niebling, J., Vinther, A., Larsen, K.P.. Numerisk modellering af plastiske betonkonstruktioner. Master's thesis; Department of civil engineering, Byg-DTU; 2007.

[31] Olsen, P.C.. The influence of the linearisation of the yield surface on the load-bearing capacity of reinforced concrete slabs. Computer methods in applied mechanics and engineering 1998;162(1-4):351–358.

[32] Papanikolaou, V.K.. Analysis of arbitrary composite sections in biaxial bending and axial load. Computers & Structures 2012;9899:33 – 54.

[33] Pastor, J., Thai, T.H., Francescato, P.. New bounds for the height limit of a vertical slope. International Journal for Numerical and Analytical Methods in Geomechanics 2000;24(2):165 – 182.

[34] Sfakianakis, M.G.. Biaxial bending with axial force of reinforced, composite and repaired concrete sections of arbitrary shape by fiber model and computer graphics. Advances in Engineering Software 2002;33(4):227–242.

[35] Skordeli, M.A.A., Bisbos, C.D.. Limit and shakedown analysis of 3d steel frames via approximate ellipsoidal yield surfaces. Engineering Structures 2010;32(6):1556–1567.

[36] Sloan, S.W.. Lower bound limit analysis using finite elements and linear programming. International Journal for Numerical and Analytical Methods in Geomechanics 1988;12(1):61–77.

[37] Sloan, S.W.. Upper bound limit analysis using finite elements and linear programming. International Journal for Numerical and Analytical Methods in Geomechanics 1989;13(3):263–282.

[38] Sloan, S.W., Kleeman, P.W.. Upper bound limit analysis using discontinuous velocity fields. Computer Methods in Applied Mechanics and Engineering 1995;127(1-4):293 – 314.

[39] Tin-Loi, F., Pang, J.S.. Elastoplastic analysis of structures with nonlinear hardening: a nonlinear complementarity approach. Computer methods in applied mechanics and engineering 1993;107(3):299–312.

[40] Vidal Codina, F.. Optimal collapse simulator for three-dimensional structures. Master's thesis; Universitat Politècnica de Catalunya; 2011.

[41] Watwood, V.B.. Mechanism generation for limit analysis of frames. Journal of the Structural Division 1979;105(1):1–15.

[42] White, D.W., Chen, W.F.. Plastic hinge based methods for advanced analysis and design of steel frames: An assessment of the State-of-the-Art. Lehigh Univ, 1993.